

Wide Voltage-Regulation Range Synchronous-Rectifier LLC Converter With Novel Operation Modes

Xiang Zhou^{ID}, Senior Member, IEEE, Jiarui Wu^{ID}, Student Member, IEEE, Huan Luo^{ID}, Member, IEEE, Zihao Song^{ID}, Long Pei^{ID}, Student Member, IEEE, Donghua Duan, Student Member, IEEE, Peng Guo^{ID}, Member, IEEE, Laili Wang^{ID}, Senior Member, IEEE, and Yan-Fei Liu^{ID}, Fellow, IEEE

Abstract—Traditionally, the energy feedback in synchronous rectifier (SR) LLC converter was once considered to only have the ability to reduce the voltage gain. In this article, a kind of special energy feedback caused by the novel operation modes of LLC resonant converter is proposed for improving voltage gain. Compared to the P, O, and N stages in conventional LLC converter, stage F is built by controlling the turn-on early time of the SR. By using the proposed operation modes, not only zero-voltage switching (ZVS) of both the primary-side and secondary-side switches is achieved, but the voltage gain of the LLC converter can be increased significantly with a narrow switching frequency range and a smaller magnetizing inductance circulating current. In addition, the proposed operation modes are simple and easy to be utilized in full bridge, half bridge, and so on; all kinds of LLC converters thus can form a new general control strategy of the SR LLC. Finally, a 100-W half-bridge SR LLC dc–dc converter prototype with a wide voltage-regulation range is implemented to validate the proposed operation modes and the theoretical analysis.

Index Terms—LLC dc–dc converter, narrow switching frequency range, synchronous rectifier (SR), wide voltage-regulation range.

I. INTRODUCTION

RECENTLY, along with the rapid development of electric vehicles (EVs), fast EV charger, on-board converter

Received 20 August 2024; revised 22 October 2024 and 22 December 2024; accepted 21 February 2025. Date of publication 26 February 2025; date of current version 24 July 2025. This work was supported in part by the National Natural Science Foundation of China under Grant 52407218 and in part by the Open Fund of the State Key Laboratory of High-Efficiency and High-Quality Conversion for Electric Power under Grant 2024KF009. (Corresponding author: Laili Wang.)

Xiang Zhou, Jiarui Wu, Zihao Song, Long Pei, Donghua Duan, and Laili Wang are with the State Key Laboratory of Electrical Insulation and Power Equipment, Xi'an Jiaotong University, Xi'an 710049, China, and also with the State Key Laboratory of High-Efficiency and High-Quality Conversion for Electric Power (e-mail: zhouxiang06@xjtu.edu.cn; wujiarui123@stu.xjtu.edu.cn; zihaosong@stu.xjtu.edu.cn; pl0823@stu.xjtu.edu.cn; 564752353@qq.com; llwang@mail.xjtu.edu.cn).

Huan Luo is with the College of Electrical Engineering, Sichuan University, Chengdu 610064, China (e-mail: luohuan2387@163.com).

Peng Guo is with the State Key Laboratory of High-Efficiency and High-Quality Conversion for Electric Power, Hunan University, Changsha 410082, China (e-mail: pengguo92@hnu.edu.cn).

Yan-Fei Liu is with the Department of Electrical and Computer Engineering, Queen's University, Kingston, ON K7L 3N6, Canada (e-mail: yanfei.liu@queensu.ca).

Digital Object Identifier 10.1109/TTE.2025.3545817

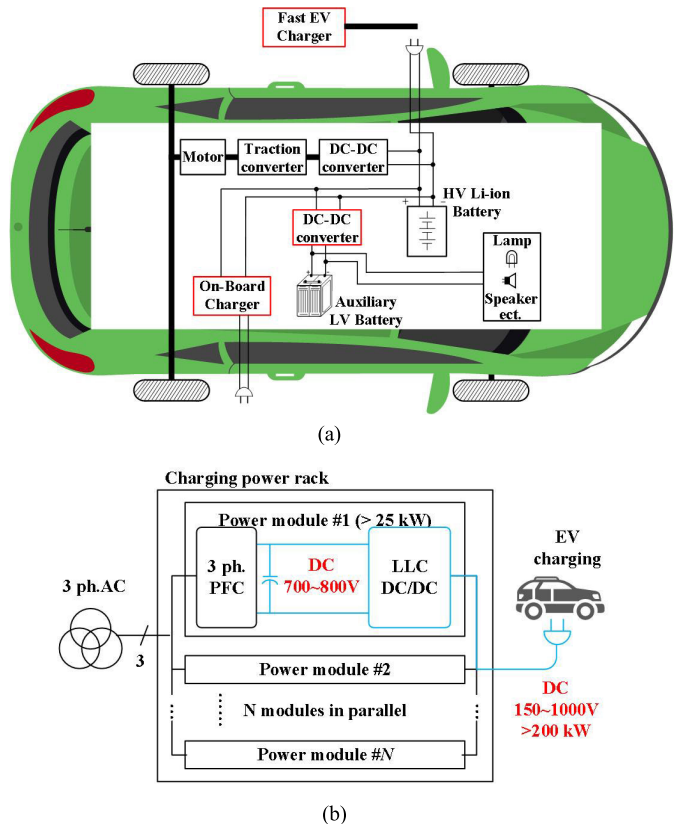


Fig. 1. Diagram of (a) EV charging power rack [1] and (b) EV power train [14].

(OBC), and on-board low-voltage dc–dc converter (LDC) are essential in EVs. Generally, EV batteries can be either 400 V (with a range of 150–500 V) or 800 V (with a range of 300–1000 V). As shown in Fig. 1(a), for OBC, an isolated dc–dc converter with a wide output voltage range of 150–500 or 300–1000 V is required. For LDC, an isolated dc–dc converter with a wide input voltage range of 150–500 or 300–1000 V is required. As shown in Fig. 1(b), in order to accommodate both 400- and 800-V batteries, the dc/dc converter in universal fast EV chargers must cover an extremely wide output voltage range, such as 150–1000 V [1]. Therefore, a high-efficiency high-power-density isolated dc–dc converter

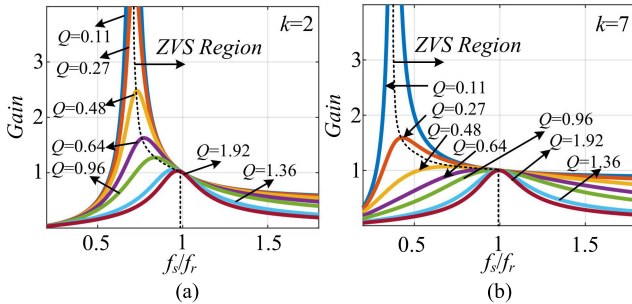


Fig. 2. Voltage gain against switching frequency with different k and Q values. (a) $k = 2$ and (b) $k = 7$.

with wide voltage regulation capability is more and more important in EVs application [2], [3], [4], [5].

LLC series-parallel resonant converter was first apparent in 1988 in [6] and [7] and attracts more and more attention since the 2000s for industrial applications and research [8], [9]. As one of the most popular isolated dc-dc converters, *LLC* resonant converter can satisfy the increasing requirement for high-efficiency and high-power-density switching mode power supply due to the simplest topology and the soft switching of the primary-side switches and secondary-side rectifiers [9]. Although *LLC* converter has many advantages, it is obviously impossible to cover the various requirement in different applications. For the wide input and/or output voltage range applications, it is challenging for the *LLC* converter to achieve wide voltage regulation capability.

Fig. 2 shows the voltage gain against switching frequency with different resonant inductance ratio k and quality factor Q based on the fundamental harmonic approximation, where k and Q are defined in [9] as follows:

$$\left\{ \begin{array}{l} k = \frac{L_p}{L_r}, \quad Q = \frac{\sqrt{\frac{L_p}{C_r}}}{R_{ac}}, \quad R_{ac} = \frac{8n^2}{\pi^2} R_o \end{array} \right. \quad (1)$$

where L_r is the series resonant inductance, C_r is the series resonant capacitance, L_p is the parallel resonant inductance, n is the turns ratio of the transformer, and R_o is the load resistance. k is generally used to describe the capability of the step-up voltage gain, and Q is generally used to describe the relationship between the load and the resonant parameters in *LLC* converter. From Fig. 2, the characteristic of the parallel resonance is more and more obvious in *LLC* converter when k is decreased, thereby obtaining a high step-up voltage gain; the characteristic of the series resonance is more and more obvious in *LLC* converter when k is increased, thereby lost the capability of the step-up voltage gain. As the pulse frequency modulation (PFM) is used to regulate the output voltage in traditional *LLC* converter, thereby causing the drawback as follows.

First, the wide normalized step-up and step-down voltage-regulation ranges are realized by the extremely wide switching frequency variation range, which brings difficulties to the design of magnetic components and driver circuits [10].

Second, from Fig. 2, along with an increased Q value, the voltage gain decreases significantly, which means that the voltage gain decreases sharply along with an increased

load. To get the peak voltage gain and improve the step-up capability, the switching frequency should be reduced to lower than f_r , where f_r is the resonant frequency between the series resonant capacitance C_r and the series resonant inductance L_r . However, if the switching frequency reaches the operating point to achieve peak voltage gain, the gain-frequency curves are prone to nonmonotonic around this point, and *LLC* converter may be operating at a hard-switching region, thereby bringing control instability issue and lost soft switching characteristic [11]. Therefore, the step-up voltage gain of *LLC* converter is limited at full-load condition.

Third, according to Fig. 2, a small k value could help to improve voltage gain and shrink the switching frequency range with the same circuit parameters and load conditions. Although a small parallel resonant inductance L_p is good for wide voltage range applications, a high circulating current and high turn-off current would cause high conduction and switching loss, thereby degrading the system efficiency of the *LLC* converter [12].

Along with the wide voltage-regulation range applications develop rapidly, such as EV chargers, power delivery (PD) adapters, photovoltaic dc-dc converters, fuel cell power systems, and so on, a single conventional *LLC* converter cannot satisfy the requirements of these applications directly as the voltage gain curve at the inductive region is very flat under heavy load and the capability of the step-up voltage gain of *LLC* converter is also weak [10], [11], [12]. Therefore, it is urgent and necessary to expand the voltage- of the *LLC* regulation capacity and enhance the competitiveness converter in wide input and/or output voltage range applications.

In [13] and [14], the operation modes of the conventional *LLC* resonant converter are analyzed and the peak gain point is present. By designing the circuit parameters with a small resonant inductance ratio k , the capacity of the step-up voltage gain can be improved slightly [15], [16]. However, a small k means a small magnetizing inductance and a high circulating current, which increases conduction loss and copper loss and degrades the converter efficiency. In [17], [18], and [19], the primary-side or secondary-side phase shift *LLC* converters are presented, and the wide voltage gain can be achieved by adjusting the phase shift angle. In these converters, the soft-switching condition is relative to the load current and phase shift angle; thus, it is difficult to achieve soft-switching under the high step-up or step-down output voltage with light load.

To achieve a higher voltage gain, some extra switches are added to *LLC* converter to form a boost cell that operates with pulsedwidth modulation (PWM) control [20], [21]. However, adding components will inevitably increase extra cost and complexity, and soft switching will be lost under PWM control strategy. Recently, the primary full-bridge (FB)/half-bridge (HB) hybrid operation modes *LLC* converter is presented to enhance the step-up voltage gain capacity [22], [23], [24]. Due to the voltage gain of FB *LLC* converter being two times that of HB *LLC* converter under resonant frequency point, by using the topology-reconfigurable primary side to make the *LLC* converter operates at different modes, the voltage-regulation range can be broadened significantly [24].

Similarly, a topology-reconfigurable secondary rectifier can also make the *LLC* converter operates at different modes to improve the voltage-regulation range [25], [26]. In these FB and HB hybrid control *LLC* converters, the FB circuit and some extra switches are required in the primary or secondary side, which increases the cost and control complexity. In addition, when the operation mode is changed between FB and HB, the switching frequency jumps sharply, which causes a large output voltage oscillation and deteriorates the dynamic characteristic. As the switching frequency of each switch is different under the different operation modes, thus the loss and the temperature among these switches are not balanced, which needs to be optimized to improve reliability and extend life [27]. In [28] and [29], the topology-reconfiguration transformers can help to improve output voltage regulation capability in *LLC* converter. However, the extra transformer or switches would increase the cost and complexity of the converter.

In decades, the synchronous rectifier (SR) technology is more and more popular in *LLC* converters to reduce the conduction loss of the secondary side and improve efficiency. As a consequence, a new degree of freedom can be adopted on SR switches. In [30], by adjusting the phase shift angle of the SR switches in *LLC* converter, the resonant inductor can be used as the boost inductor, and the output voltage gain is improved along with an increased equivalent duty cycle in boost cell. However, the zero-voltage switching (ZVS) turn-on of the SR switches is lost by using this scheme, which increases the secondary-side switching loss. In [31], [32], and [33], the control scheme that makes turn-off time delay of SR switches is proposed, which results that the energy is transformed to the primary side, and the ZCS turn-off of the SR switches is lost by using this scheme.

In this article, the novel operation modes of *LLC* converter are proposed by controlling the turn-on early time of SR to achieve the energy feedback and high-voltage gain with ZVS turn-on and ZCS turn-off of SR switches, which are suitable for the wide voltage-regulation range applications. The novelty and the advantages of the proposed *LLC* converter lie in: 1) the novel operation modes consisting of stage F are proposed and elaborated; 2) without any adding components, the voltage gain is increased significantly along with an increasing leading angle of SR switches. Therefore, by the proposed novel operation modes, the switching frequency range is squeezed significantly, which is good for the design of the magnetic components. Compared to the conventional *LLC* converter, the large magnetizing inductance could be designed to reduce the circulating current if the same voltage gain is required; 3) soft switching can be achieved in the primary sides easily due to the higher current through the resonant inductor when the primary switches are turned off; 4) soft switching can be achieved in the secondary sides due to voltage ringing across the SRs; 5) the peak voltage of the resonant capacitor and the peak currents of the transformer primary and secondary winding are reduced when the switching frequency is smaller and far away from the resonant frequency, which can reduce the stress of the devices; and 6) the advantages of conventional *LLC* converter are kept, such as simple circuit

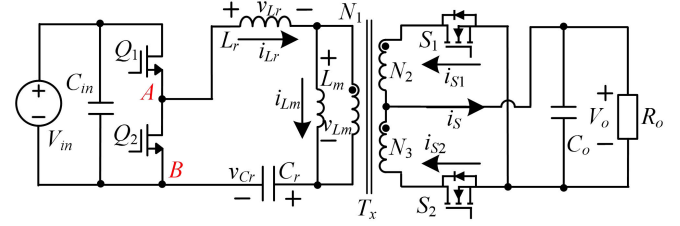


Fig. 3. HB SR *LLC* converter.

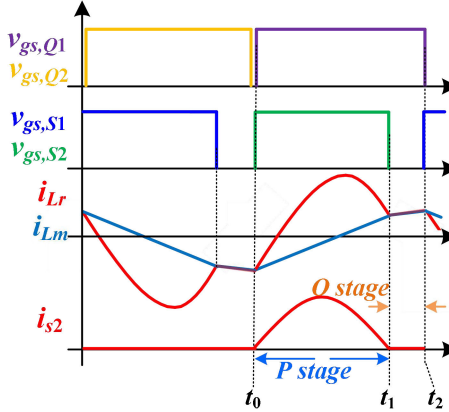


Fig. 4. Operation waveforms of the conventional *LLC* converter.

structure and control strategy, the same switching frequency among the switches and the balanced loss, and the proposed operation modes are easy to be used in all kinds of SR *LLC* converter.

II. NOVEL RESONANT STAGE OF SR *LLC* CONVERTER

In the conventional SR *LLC* converter, the operation modes consisting of P, O, and N stages have been studied and made a detailed analysis [11], [12]. From [11], OPO, PO, PON, NP, PN, and NOP are the six major operation modes in *LLC* converter, generally. To achieve high efficiency and soft switching, PO mode is the popular design for the *LLC* converter [11]. The half-bridge SR *LLC* converter is shown in Fig. 3, and the turns ratio of the transformer is $N_1:N_2:N_3 = n:1:1$, where N_1 is the turns of the primary winding and N_2 and N_3 are the turns of the secondary windings. The key waveforms of the conventional SR *LLC* converter with PO mode are shown in Fig. 4, where i_{Lr} is the current flowing through the series resonant inductance and i_{Lm} is the current flowing through the parallel resonant inductance (the magnetizing inductance of the transformer L_m is generally used as the parallel resonant inductance L_p in *LLC* converter).

According to [11], when Q_1 is turned on and Q_2 is turned off, there are P, O, and N three resonant stages depending on the voltage across the magnetizing inductor, as shown in Fig. 5(a)–(c). In a traditional *LLC* converter, the energy is always transferred from input to output in P stage or N stage or no energy is transferred to output in O stage; thus, the resonant stages only depend on the voltage across the magnetizing inductor.

However, when the active switches in SR are employed with adjustable freedom, the operation modes of the *LLC* converter

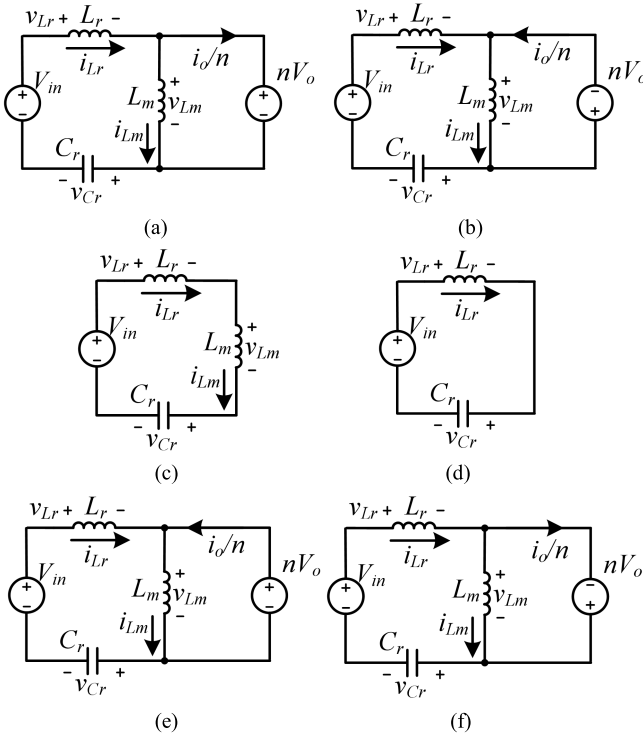


Fig. 5. Equivalent circuits of the different operation stages in LLC converter. (a) P stage. (b) N stage. (c) O stage. (d) Operation stage in [30]. (e) Operation stage in [31]. (f) Proposed F stage.

could be changed. The energy can be stored in the primary inductor or feedbacked from output to input, and the resonant stages depend on the voltage across the magnetizing inductor and the current flowthrough the load. Thus, the different operation stages in LLC converter are shown in Fig. 5.

According to [30], when the LLC converter operates at P or N stage, the transformer secondary can be shorted by the SR switches; thereby, the resonant inductor is charged and the energy is stored in the resonant inductor. Therefore, the conventional P or N stage can be converted to the operation stage in [30] by using SR switches, which is shown in Fig. 5(d).

When the LLC converter operates from P stage to O stage, the SR switches should have been turned off. However, if the SR switches are turned off delay, the conventional O stage is converted to the operation stage in [31]. The equivalent circuit is shown in Fig. 5(e), and the key waveforms are shown in Fig. 6. As SR switches are turned off at time t_1 instead of t_0 when the switching frequency of the LLC converter is lower than the resonant frequency, the energy is feedbacked from output to input; thus, the voltage gain is reduced. Although ZCS turn-off of the SR switches is lost by using these schemes, the high step-down voltage regulation capability is obtained. Consequently, the energy feedback in SR-LLC converter was once considered traditionally only to have the ability to reduce the voltage gain.

In [34], the voltage ringing across SR switches is elaborated. However, the effect of turn-on early of SR switches is not analyzed, and the circuit parameters design method is just given to avoid the turn-on early of SR switches in [34].

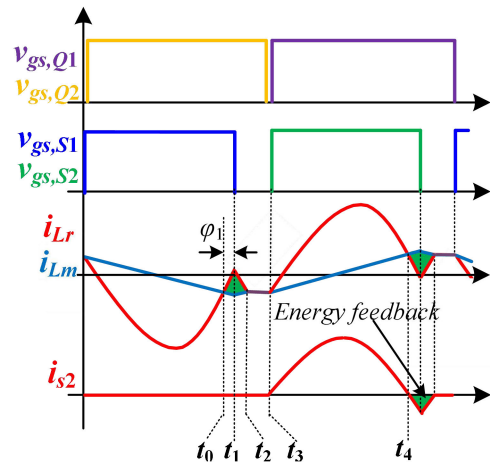


Fig. 6. Operation waveforms of the LLC converter in [31].

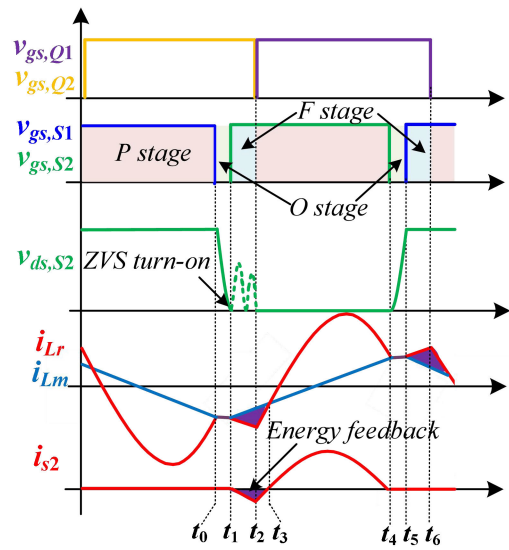


Fig. 7. Key waveforms of the HB SR LLC converter with F stage.

Thus, it is considered traditionally that only can reduce the voltage gain and cause a large circulating current to deteriorate the efficiency. Based on the effort in [34], the effect of turn-on early of SR switches is elaborated in this article. The research effort shows that the voltage gain can be improved, the soft-switching characteristics of all the switches can be kept by turn-on early of SR switches, and the efficiency is not always reduced, which is totally different from the conventional wisdom.

Fig. 7 shows the key waveforms of the proposed HB SR LLC converter with F stage. During t_0-t_2 , the SR switch S_2 is turned on at t_2 in the conventional LLC converter, and the period t_0-t_2 is defined as O stage. If the SR switch S_2 is turned on early at t_1 , O stage is reduced from t_0-t_2 to t_0-t_1 . The energy is feedbacked from output to input, and the load current flows out of load during t_1-t_2 . Thus, the operation during t_1-t_2 is defined as F stage in this article, and the conventional O stage during t_1-t_2 is converted to F stage. Here, $\alpha = 360^\circ \times (t_2 - t_1)/T_s$ represents the SR switches leading angle. The equivalent circuit of F stage is shown in Fig. 5(f). As a

sequence, the current i_{Lr} is increased by F stage, and ZVS turn-on of switches Q_1 and Q_2 can be achieved easily at t_6 and t_2 due to a higher current i_{Lr} .

As aforementioned analysis, O stage can be converted to F stage by turn-on early of SR switches. However, along with the load current increased, if N stage occurs, F stage would be lost and is the same as N stage. Therefore, F stage is degenerated to N stage, because SR switches should have been conducted early at N stage.

In the traditional SR LLC converter, the voltage across SR switches is not zero during t_0-t_2 ; thus, the turn-on early of SR switches will lose ZVS, causing high switching loss. In [34], by designing the circuit parameters properly, the voltage ringing across SR switches could help to achieve ZVS during t_0-t_2 . As shown in Fig. 7, when the voltage ringing reaches zero at t_1 , turn-on early switch S_2 can achieve ZVS. According to [34], the voltage across SR switches $v_{ds,S2}$ during t_0-t_2 can be expressed as

$$\begin{aligned} v_{ds,S2}(t - t_0) &= \frac{V_o}{2} - \frac{K}{2n(K+1)} \\ &\times \left[\left(-2nV_o + V_{in} + \frac{V_o^2}{4C_r R_o V_{in} f_s} \right) \cos \omega_p(t - t_0) \right. \\ &\quad \left. + \frac{nV_o \pi \sqrt{K+1}}{2K} \sin \omega_p(t - t_0) \right] \\ &+ \left[\frac{V_o}{2} + \frac{K}{2n(K+1)} \right. \\ &\quad \left. \times \left(-2nV_o + V_{in} + \frac{V_o^2}{4C_r R_o V_{in} f_s} \right) \right] \cos \omega_h(t - t_0) \quad (2) \end{aligned}$$

where K , ω_r , ω_p , and ω_h satisfy

$$\begin{cases} \omega_h = \frac{1}{\sqrt{\frac{L_r L_m}{(L_r + L_m)} \times \frac{C_{oss} + C_p}{n^2}}} \\ \omega_p = \frac{1}{\sqrt{(L_r + L_m) C_r}}, \quad K = \frac{L_m}{L_r}, \quad \omega_r = \frac{1}{\sqrt{L_r C_r}} \end{cases}$$

where C_p is the parasitic paralleled capacitance of the transformer and C_{oss} is the parasitic output capacitance of the SR switches. Hence, ZVS of SR switches can be guaranteed by a simple circuit parameters design.

Fig. 8 shows the qualitative diagram of the apparent input power of LLC converter with SR switches turn-off delay or turn-on early. A_Q represents the area enclosed by the current i_{Lr} and time axis. Where T_s is the switching period, P_o is the active output power, and Q_{Lm} is the reactive power caused by the magnetizing inductor. The following assumptions are made: 1) the active power $P_{in} = P_o$; 2) Q_{Lm} is the same in the three operation modes, as shown in Fig. 8; and 3) the current i_{Lm} is the same at the end of P stage in the three operation modes, as shown in Fig. 8.

Therefore, in the conventional LLC converter, when switch Q_2 is conducted, the apparent input power of LLC converter S_{in} can be expressed as in (3). From Fig. 8, compared to the conventional LLC converter, the apparent input power S_{in} is reduced by the SR switches turn-off delay, because the area enclosed by the current i_{Lr} and time axis is reduced by A_E . Compared to the conventional LLC converter, the apparent

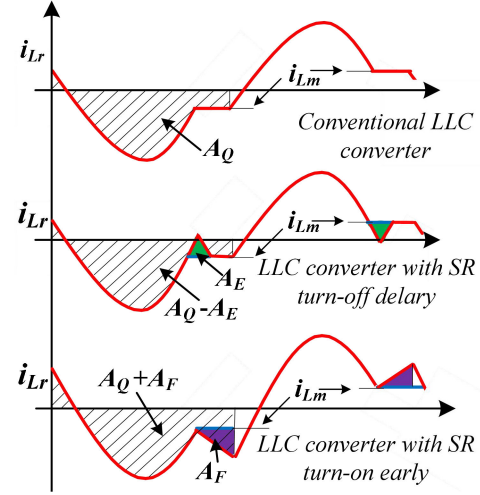


Fig. 8. Qualitative diagrams of the apparent input power of LLC converter with SR switches turn-off delay or turn-on early.

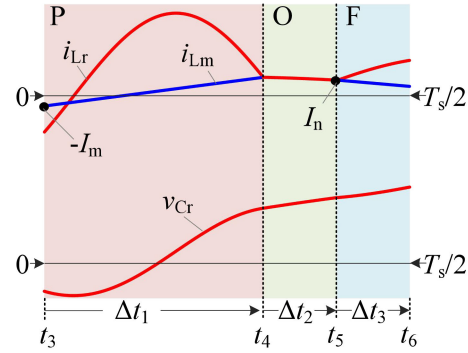


Fig. 9. Waveforms of POF mode.

input power S_{in} is increased by the SR switches turn-on early, because the area enclosed by the current i_{Lr} and time axis is increased by A_F

$$\begin{aligned} S_{in} &= \frac{V_{in} \times 2 \int_0^{T_s/2} i_{Lr} dt}{T_s} = \frac{2V_{in} A_Q}{T_s} \\ &= \sqrt{P_o^2 + Q_{Lm}^2} = \sqrt{\left(\frac{V_o^2}{R_o}\right)^2 + Q_{Lm}^2}. \quad (3) \end{aligned}$$

As a qualitative result, according to (3), the output voltage is increased when the SR switches are turned on early, and the output voltage is decreased when the SR switches are turned off delay.

As only O stage can be modified as F stage and PO mode is the most favorable operation mode of the LLC [11], the PO mode is selected as an example to analyze in this article.

III. OPERATION MODES AND CHARACTERISTIC ANALYSIS

A. Operation Modes and Voltage Gain Analysis

Fig. 9 shows the waveforms of POF mode within the positive half switching cycle (t_2-t_6 in Fig. 7).

During state P, the current flowing through resonant inductor L_r and magnetizing inductor L_m , as well as the voltage across

the resonant capacitor C_r can be described as

$$\begin{cases} i_{LrP}(t) = I_{LrP} \sin(\omega_r t - \varphi_P) \\ i_{LmP}(t) = -I_m + \frac{NV_o}{L_m} t \\ v_{CrP}(t) = v_{ab} - NV_o - L_r \frac{di_{LrP}}{dt} \end{cases} \quad (4)$$

where I_{LrP} and φ_P are the magnitude and initial phase angle of i_{LrP} , respectively, $-I_m$ is the initial current of i_{LmP} , $\omega_r = 1/(L_r C_r)^{1/2}$ is the angular frequency of series resonance of L_r and C_r , N is the turn ratio of the transformer, and v_{ab} is the voltage of the resonant tank, which is equal to V_{in} .

During state O, L_m joins the resonance of L_r and C_r , and the resonant variables can be obtained as

$$\begin{cases} i_{LrO}(t) = I_{LrO} \sin(\omega_m t - \varphi_O) \\ i_{LmO}(t) = i_{LrO}(t) \\ v_{CrO}(t) = v_{ab} - (L_r + L_m) \frac{di_{LrO}}{dt} \end{cases} \quad (5)$$

where I_{LrO} and φ_O are the magnitude and initial phase angle of i_{LrO} , respectively, and $\omega_m = 1/((L_r + L_m)C_r)^{1/2}$ is the angular frequency of series resonance of L_r , L_m , and C_r .

During state F, the corresponding resonant variables can be obtained as

$$\begin{cases} i_{LrF}(t) = I_{LrF} \sin(\omega_r t - \varphi_F) \\ i_{LmF}(t) = I_n - \frac{NV_o}{L_m} t \\ v_{CrF}(t) = v_{ab} + NV_o - L_r \frac{di_{LrF}}{dt} \end{cases} \quad (6)$$

where I_{LrF} and φ_F are the magnitude and initial phase angle of i_{LrF} , respectively, and I_n is the initial current of i_{LmF} .

When the converter moves from one state to its adjacency state, the current through the resonant inductor and the voltage across the resonant capacitor cannot change suddenly. Therefore, the continuity condition for the resonant current can be expressed as

$$\begin{cases} i_{LrP}(\Delta t_1) = i_{LrO}(0) \\ i_{Lrm}(\Delta t_1) = i_{LrO}(0) \\ i_{LrO}(\Delta t_2) = i_{LrF}(0) \\ i_{LrO}(\Delta t_2) = i_{LmF}(0) \end{cases} \quad (7)$$

where Δt_1 , Δt_2 , and Δt_3 are the durations of state P, state O, and state F, respectively, which meet

$$\Delta t_1 + \Delta t_2 + \Delta t_3 = T_s/2. \quad (8)$$

Similarly, the continuity condition for the resonant capacitor voltage can be expressed as

$$\begin{cases} v_{CrP}(\Delta t_1) = v_{CrO}(0) \\ v_{CrO}(\Delta t_2) = v_{CrF}(0). \end{cases} \quad (9)$$

By the symmetry of the half-bridge LLC converter, the end value of the current should be opposite to the initial value within a half switching cycle. Therefore, the symmetry condition for the resonant current and the magnetizing current can be described as

$$\begin{cases} i_{LrP}(0) + i_{LrF}(\Delta t_3) = 0 \\ i_{LmP}(0) + i_{LmF}(\Delta t_3) = 0. \end{cases} \quad (10)$$

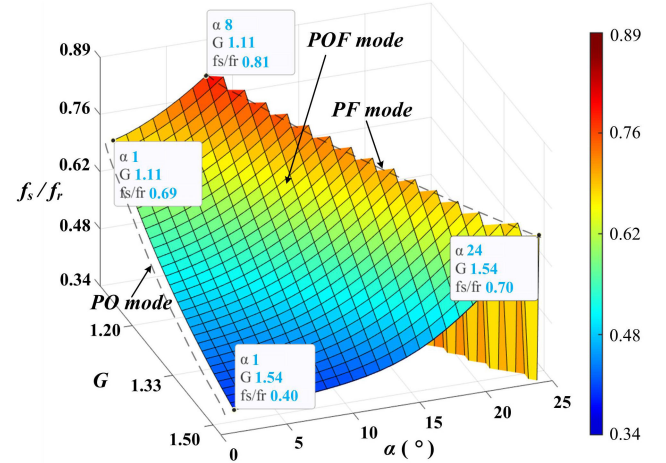


Fig. 10. Relationship among the voltage gain, switching frequency, and the SR switches leading angle.

For the symmetry condition for resonant capacitor voltage, the sum between the end value and the initial value of v_{Cr} should be equal to v_{ab} within a half switching cycle

$$v_{CrP}(0) + v_{CrF}(\Delta t_3) = v_{ab}. \quad (11)$$

The average current following through switch Q_1 over one switching cycle is equal to the input current; thus, the input power can be obtained as

$$P_{in} = V_{in} \cdot I_{in} = \frac{V_{in}}{T_s} \left(\int_0^{\Delta t_1} i_{LrP} dt + \int_0^{\Delta t_2} i_{LrO} dt + \int_0^{\Delta t_3} i_{LrF} dt \right). \quad (12)$$

The output power can be similarly obtained as

$$P_o = \frac{2NV_o}{T_s} \left[\int_0^{\Delta t_1} (i_{LrP} - i_{LmP}) dt + \int_0^{\Delta t_3} (i_{LmF} - i_{LrF}) dt \right]. \quad (13)$$

The assumption of $P_{in} = P_o$ is made. Then, by substituting (3)–(5) into (6)–(12) and taking V_o , V_{in} , P_o , and Δt_3 as known parameters, 12 transcendental equations can be obtained to solve for the corresponding switching frequency f_s , as well as other current and voltage variables, including I_{LrP} , I_{LrO} , I_{LrF} , I_m , I_n , φ_P , φ_O , φ_F , Δt_1 , and Δt_2 . Therefore, the voltage gain of the SR LLC converter with POF mode can be shown in Fig. 10. When the SR switches leading angle α is zero, the LLC converter operates at conventional PO mode. Along with the leading angle α increasing, O stage is reduced and modified as F stage, and the voltage gain is increased gradually at the same switching frequency. Finally, the whole O stage is modified as F stage, and the converter operates at PF mode.

B. Circuit Characteristic Analysis

When the resonant components are $L_r = 10 \mu\text{H}$, $L_m = 120 \mu\text{H}$, $C_r = 120 \text{nF}$, the turns ratio of the transformer is 5:1:1, the output voltage is 12 V, and the load current is 8 A, the relationship among the voltage gain, switching frequency,

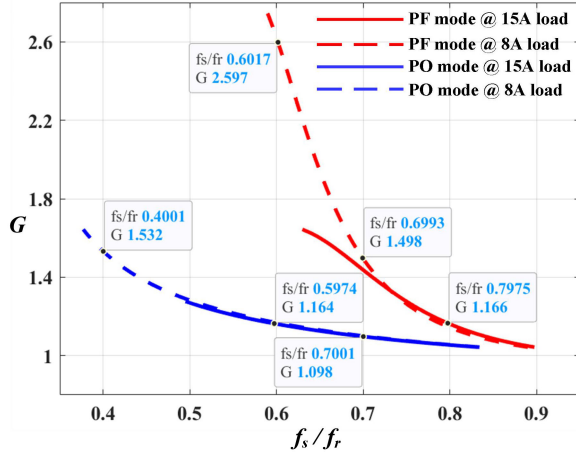


Fig. 11. Comparison of the voltage gain between PO and PF modes.

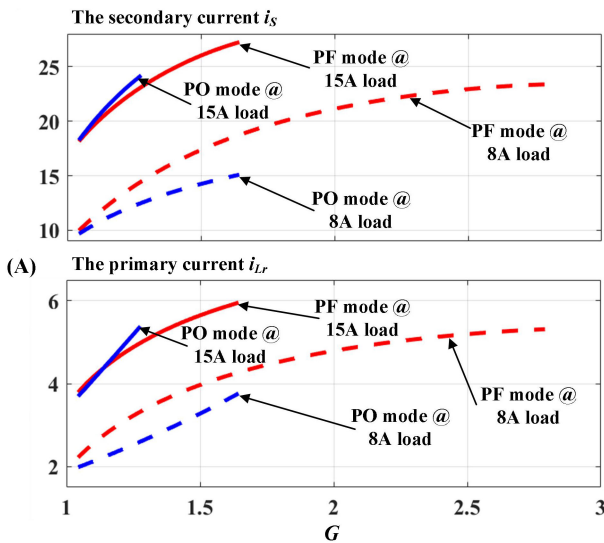


Fig. 12. Comparison of the rms current between PO and PF modes.

and the SR switchers leading angle is shown in Fig. 10, and the comparisons of the voltage gain and current between PO and PF modes are shown in Figs. 11 and 12. The peak voltage and current comparisons are shown in Fig. 13.

As shown in Fig. 11, when the load current is 8 A, the voltage gain of the LLC converter operating at PF mode is 2.23 times of that at PO mode at $f_s/f_r = 0.6$, and the switching frequency range of the PF mode LLC converter is 50% reduced compared to PO mode LLC converter at around the voltage gain $G = 1.5$. Moreover, the voltage gain can reach to $G = 2.74$ at PF mode, but only 1.64 is obtained at PO mode even though the switching frequency is much lower.

From Fig. 12, the primary and secondary currents in the PO mode are slightly smaller than that in PF mode under 8-A load current. However, along with the load current increasing, the switching frequency is required to be far away from the resonant frequency f_r to keep the same voltage gain in LLC converter. As a consequence, the time interval of P stage is reduced and the O stage is extended. Therefore, the peak value of the primary and secondary current is increased significantly

to ensure that the average value of secondary current i_s is equal to the load current, which causes a high root mean square (rms) value of the primary and secondary currents in the LLC converter with PO mode; thereby, the conduction loss increased. As shown in Fig. 9, although there is feedback current during F mode, the time interval of energy transferred into the secondary side is still increased as O stage is reduced. Hence, the rms currents of the primary and secondary sides are even smaller than that in PO mode under heavy load and low switching frequency, such as 15-A load current in when input voltage against (a) switching frequency (b) leading angle α .

From (4)–(13), the time-domain model of the LLC converter is established; thus, the comparison of the LLC converter under PO and PF mode when input voltage against (a) switching frequency, (b) leading angle α , (c) the peak resonant current $i_{Lr,\max}$, (d) the peak magnetizing current $i_{Lm,\max}$, (e) the peak secondary-side current $i_{s,\max}$, and (f) the peak resonant voltage $v_{Cr,\max}$ is shown in Fig. 13. It can be seen that not only the more narrow switching frequency range and the wider input voltage regulation range are achieved, but the peak values of the current flow through the magnetizing inductor, the current flows through the primary-side resonant inductor, the current flows through the secondary-side SR switches, and the voltage across primary-side resonant capacitor in PF mode is lower than that in conventional PO mode along with the input voltage decreased.

Although the rms current in PF mode is slightly higher than that in PF mode at 8-A load current from Fig. 12, the current stress of the primary and secondary-side switches, and the voltage stress of the resonant capacitor can be reduced by the lower peak value of the primary- and secondary-side current and resonant voltage v_{Cr} from Fig. 13.

In LLC converter, the flux density in the high-frequency transformer is a function of magnetizing current and can be expressed as

$$L_m i_{Lm\max} = N_{Tp} B_{\max,Lm} S_T \quad (14)$$

where L_m is the inductance value of the magnetizing inductor, $i_{Lm\max}$ is the maximum value of the magnetizing current, N_{Tp} is the primary winding turns number, $B_{\max,Lm}$ is the peak ac flux density of the magnetizing inductor, and S_T is the cross-sectional area of the middle leg of the transformer core.

The flux density in the resonant inductor is a function of the primary current and can be expressed as

$$L_r i_{Lr\max} = N_{Lr} B_{\max,Lr} S_{Lr} \quad (15)$$

where L_r is the inductance value of the resonant inductor, $i_{Lr\max}$ is the maximum value of the primary current, N_{Lr} is the turns number of the resonant inductor L_r , $B_{\max,Lr}$ is the peak ac flux density of the resonant inductor, and S_{Lr} is the cross-sectional area of the middle leg of the resonant inductor core.

The common approach that characterizes core losses is the empirical Steinmetz equation, which is expressed as

$$P_v = k \cdot f_s^\alpha \cdot (B_{\max})^\beta \quad (16)$$

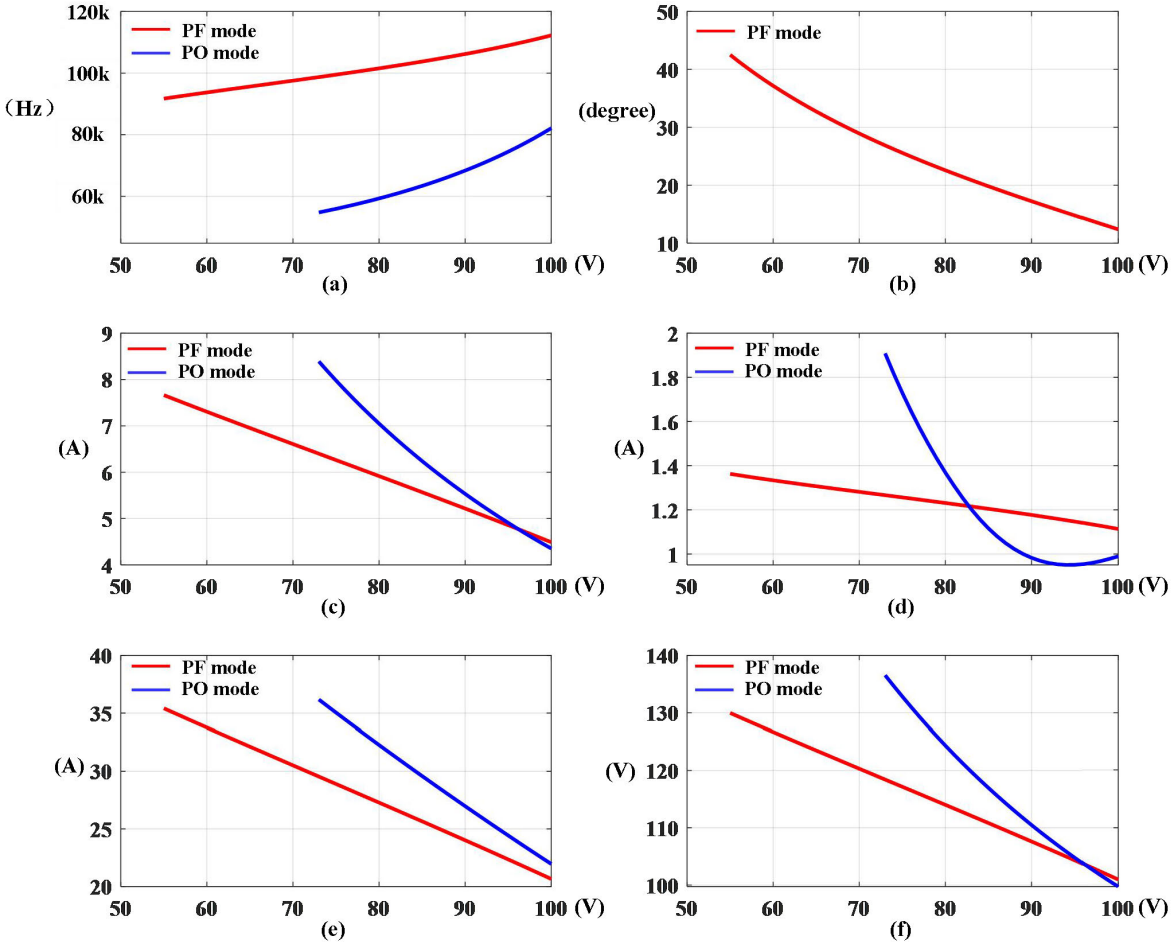


Fig. 13. When $L_r = 10 \mu\text{H}$, $L_m = 120 \mu\text{H}$, and $C_o = 120 \text{nF}$, the turns ratio of the transformer is 5:1:1, 12-V/8-A output, (c) peak resonant current $i_{Lr,\max}$, (d) peak magnetizing current $i_{Lm,\max}$, (e) peak secondary-side current $i_{s,\max}$, and (f) peak resonant voltage $v_{Cr,\max}$.

where k , α , and β are constants provided by the manufacturer, and P_v is the time-average core loss per unit volume with switching frequency f_s .

From (14)–(16), the peak ac flux density $B_{\max,Lr}$ is proportional to the current i_{Lr} , and the peak ac flux density $B_{\max,Lm}$ is proportional to the current i_{Lm} . From [35], the coefficient α for ferrite materials N87 is 1.63, and the coefficient β for ferrite materials N87 is 2.25. According to Fig. 13, if input voltage is 75 V, the core loss of the transformer and the resonant inductor of the proposed converter is around 1.2–1.4 times higher than that of the conventional LLC converter as the switching frequency is reduced from 100 to 60 kHz. Nevertheless, from [40], the output voltage ripple of LLC converter can be calculated as

$$\Delta v_o = R_{\text{ESR},C_o} \times \left(\frac{\pi}{2} - 1\right) \times I_o + \frac{0.363I_o}{C_o \times f_s} \quad (17)$$

where I_o is the average output current, C_o is the output capacitance value, and f_s is the switching frequency. If the switching frequency is decreased from 100 to 60 kHz, a 1.67 times larger output capacitor is required to keep the same output voltage ripple. Meanwhile, a low switching frequency would also cause a larger size of the EMI filtering stage.

C. Closed-Loop Characteristic Analysis

As shown in Figs. 10 and 11, the gain-frequency curve is monotonous by adopting the proposed F mode; thus, the closed-loop control can be achieved in the practical applications. To verify the proposed novel operation mode in LLC converter can work with a closed loop, the logic of the closed-loop control strategy is established, which is shown in Fig. 14.

From Fig. 7, to keep achieving ZVS turn-on of the switches, the leading angle α is the discrete variable. To simplify the closed-loop control strategy, the SR switches are turned on with ZVS when the first voltage ringing reaches to zero in the practical applications by detecting the voltages across SR switches. At this case, O stage is very short and can be neglected, and the LLC converter can be regarded as operating at PF mode.

As shown in Fig. 14, when the voltage $v_{ds,S2}$ decreases to the forward voltage of body diodes $-V_F$ caused by the voltage ringing at the end of the P stage, the voltage $v_{ds,S2}$ is lower than the threshold voltage $V_{\text{TH},\text{on}}$; then, the switch S_2 is turned on at least a set value $T_{\text{on_min}}$. After $T_{\text{on_min}}$, the secondary-side current flows from source to drain of the switch S_2 , and the voltage across switch S_2 is negative. Along with the transformer secondary current decreasing to zero, the voltages

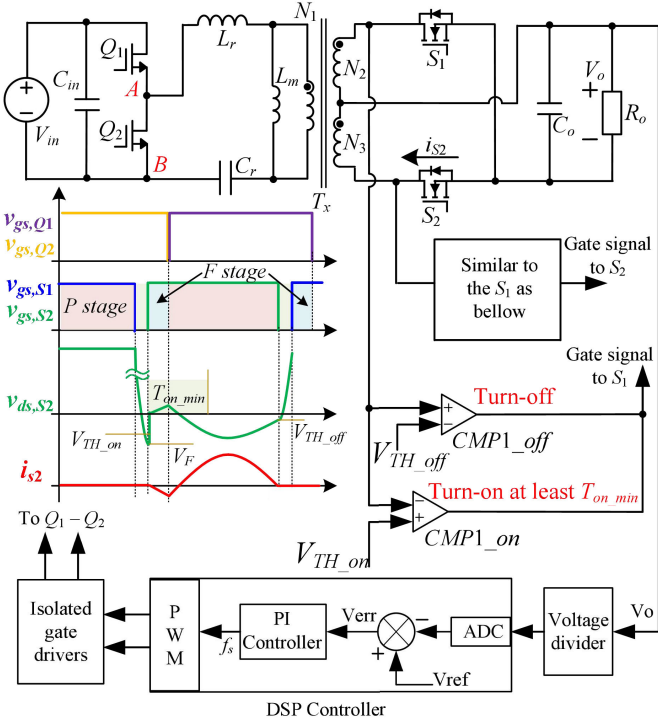


Fig. 14. Closed-loop control strategy of the proposed LLC converter with PF mode.

across SR switches are increased and higher than the threshold voltage $V_{TH,off}$ eventually; then, the switch S_2 is turned off.

According to the control strategy shown in Fig. 14, the simulated closed-loop circuit is built by using PSIM. The dynamic simulated waveforms with the load current step-up from 8 to 10 A are given in Fig. 15. As a sequence, the switching frequency is decreased from 93.2 to 91.4 kHz, the overshoot of the output voltage is less than 1 V, and the output voltage is recovered in 1 ms.

Therefore, the correction and effectiveness of the closed-loop control strategy shown in Fig. 14 can be verified by the simulated results in Fig. 15.

In summary, since the proposed scheme can improve the voltage-regulation range for the SR half-bridge or full-bridge LLC converter without any topology modification, the converter can be worked at conventional PO mode to keep the high efficiency when a low step-up gain is required or the switching frequency is closing to the resonant frequency. In scenarios with heavy loads and a requirement for high step-up voltage gain, if the voltage-regulation range exceeds the capacity of a traditional LLC converter, the converter can be operated in PF mode using the proposed scheme to cover the wide voltage-regulation range. This negates the necessity of employing two-stage converters or adding auxiliary switches to enhance the voltage-regulation capability. In this article, the analysis of the novel operation mode of LLC converter is focused on, thus, the optimal control strategy, including the transition between PF mode and PO mode, small-signal model, digital-control method, and so on, would be studied in the future work.

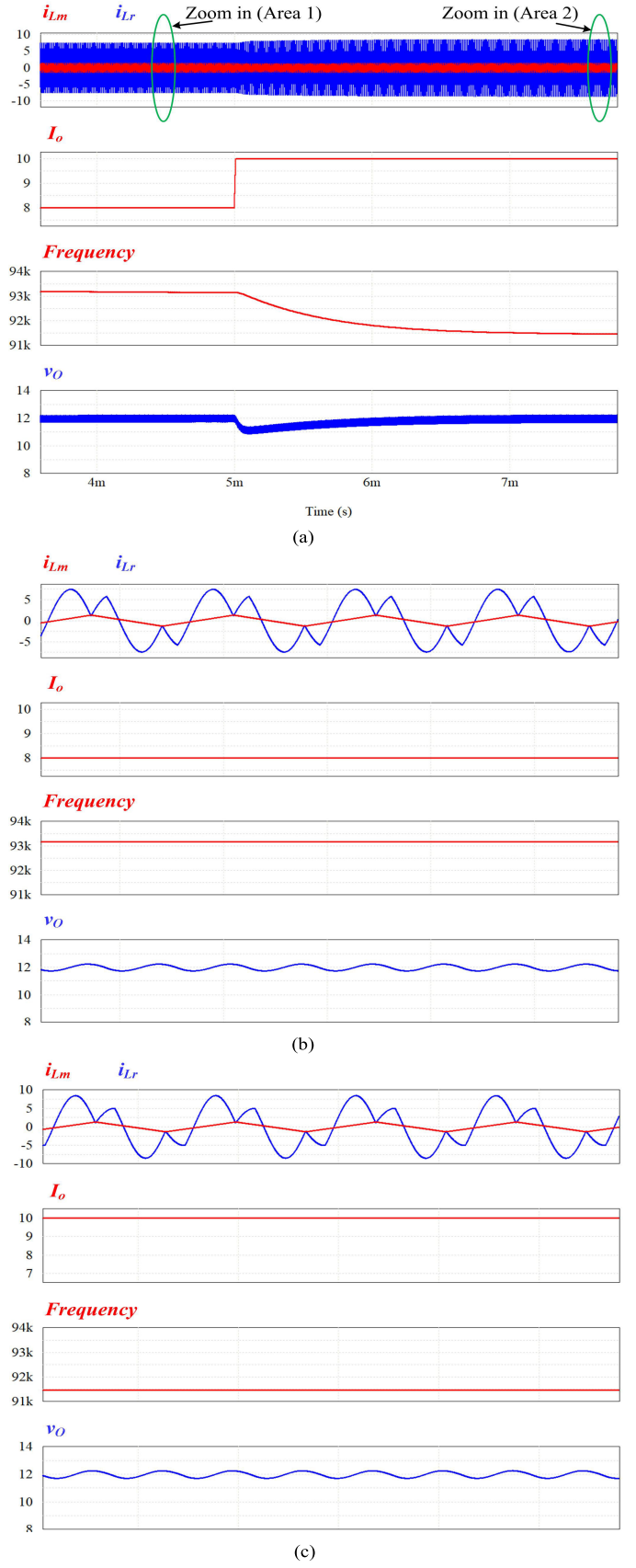


Fig. 15. Simulated closed-loop verification when $L_r = 10 \mu\text{H}$, $L_m = 120 \mu\text{H}$, $C_r = 120 \text{nF}$, $V_{in} = 60 \text{V}$, and $V_o = 12 \text{V}$. (a) Dynamic characteristic of the load current step-up from 8 to 10 A, (b) steady characteristic with 8-A load current, and (c) steady characteristic with 10-A load current.

TABLE I
SPECIFICATION AND CIRCUIT PARAMETERS OF THE PROTOTYPE

Designators	Part number/Value
Input	54V~115V
Output	12V / 8A
Switching frequency range	87kHz~132kHz
$Q_1 \sim Q_2$	BSC093N15NS5
Primary dead time	200ns
$S_1 \sim S_2$	BSC010N04LS6
Transformer	20: 4: 4, RM12 core, and N87 material, AWG20 Litz wire for the primary winding, AWG18 Litz wire for the secondary winding
L_m	118.3μH
L_r	9.8μH, RM12 core, and N87 material, AWG18 Litz wire
C_r	68nF+47nF+10nF (5% tolerance)
C_{in}	10μF×3+56μF
C_o	10μF×6+56μF
Controller	TMS320F280048
Driver	SI8233AD-D-IS

IV. EXPERIMENTAL VERIFICATION

From the aforementioned analysis, an SR *LLC* converter prototype is established to verify the theoretical analysis. The specification and the circuit parameters are shown in Table I.

Fig. 16 shows the switches Q_2 and S_1 and current i_{Lr} experimental waveforms of the SR *LLC* converter at the same output voltage and switching frequency. From Fig. 16(a) and (b), the converter operates at PF mode with 29° leading angle, and ZVS turn-on can be achieved on the primary side and secondary side, such as the switches Q_2 and S_1 . From Fig. 16(c) and (d), the converter operates at PF mode with 19° leading angle, and ZVS turn-on can be achieved on the primary side and secondary side, such as the switches Q_2 and S_1 . However, the leading angle is reduced from 29° to 19° at F mode, and the input voltage increased from 75 V in Fig. 16(a) and (b) to 85 V in Fig. 16(c) and (d). As a sequence, the voltage gain can be increased along with the increased leading angle α , which is consistent with the theoretical analysis.

From Fig. 16, to achieve ZVS turn-on of the secondary-side switches, the leading angle α is discontinuous as the SR switches should be turned on at the voltage ringing reaches zero. To simplify the complexity of the control strategy, the SR switches are turned on at the first zero voltage ringing even though the leading angle α could be used as a free variable, which means the proposed *LLC* converter operates at PF mode and adopts PFM modulation strategy in this article. Since the turn-on time sensing of secondary-side switches in the proposed *LLC* converter is similar to the controller in [36], [37], [38], and [39], therefore, the new operation mode is focused on, and theoretical analysis is presented in this work.

According to the analysis in [34], the voltage ringing depends on the variables L_p , C_r , C_e , R_o , and f_s from (2). The voltage ringing across SR switches will reach zero during the O stage along with an increasing load current (decreasing load resistor R_o) [34]; thereby, ZVS turn-on of SR switches

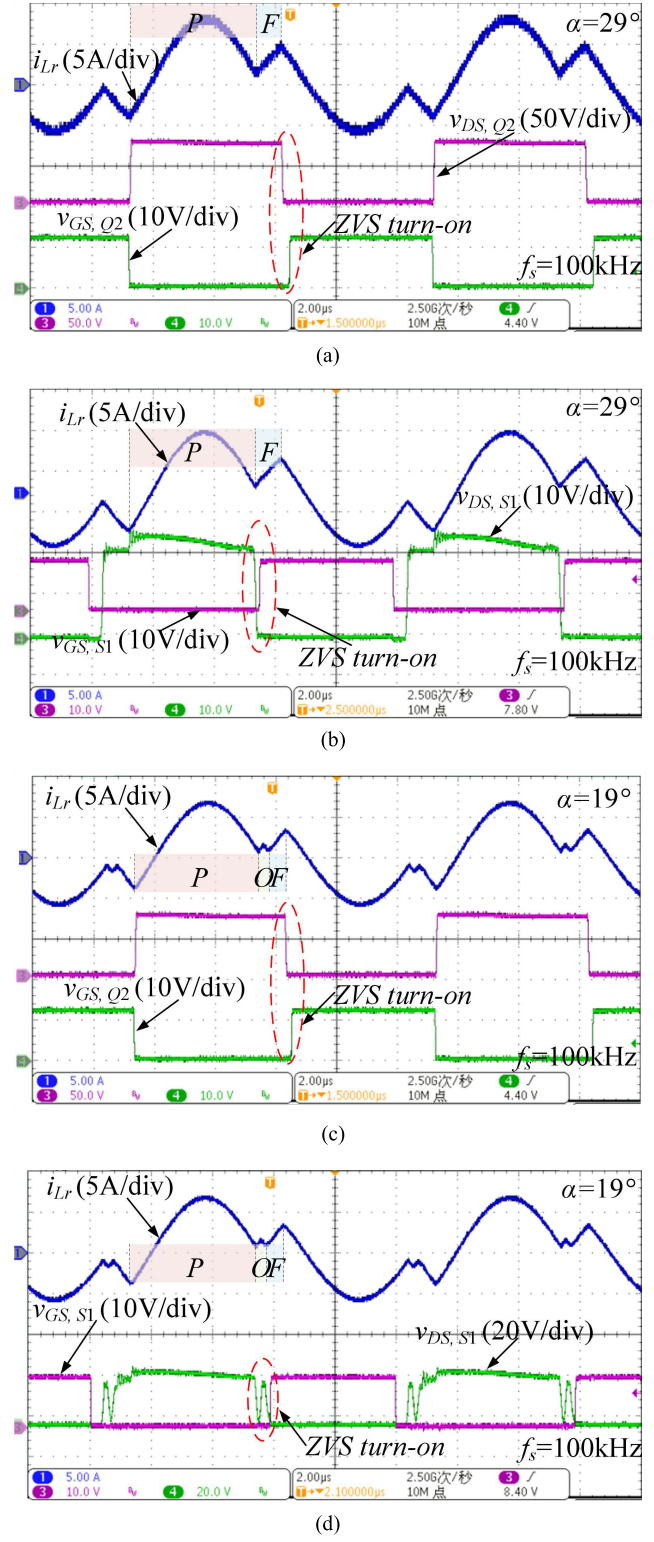


Fig. 16. Experimental waveforms at 100-kHz switching frequency at (a) and (b) $V_o = 12 \text{ V}/8 \text{ A}$ and $V_{in} = 75 \text{ V}$, (c) and (d) $V_o = 12 \text{ V}/8 \text{ A}$ and $V_{in} = 85 \text{ V}$, and (e) $V_o = 12 \text{ V}/6 \text{ A}$.

can be achieved under heavy-load conditions. However, the voltage ringing is almost higher than zero under light-load conditions with a conventional *LLC* circuit parameter design. Thereby, it is difficult to achieve full ZVS turn-on of SR switches under light-load conditions, as shown in Fig. 16(e).

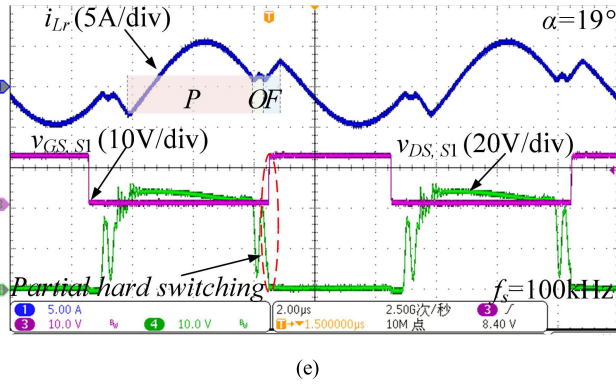


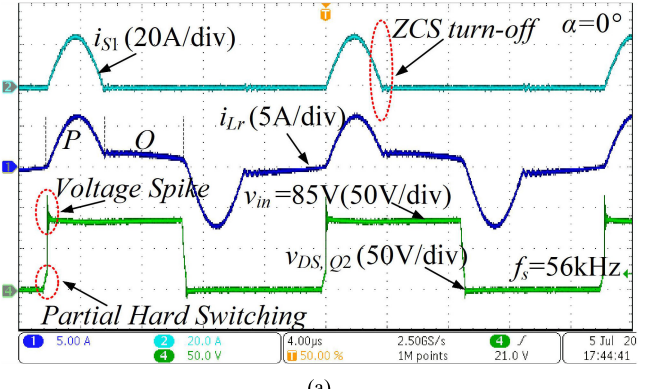
Fig. 16. (Continued.) Experimental waveforms at 100-kHz switching frequency at (e) $V_o = 12$ V/6 A.

In this case, the benefits derived from the PF mode will be significantly diminished, even the characteristics of the voltage gain, switching frequency range, and so on, shown in Fig. 13, are still better than the traditional PO mode.

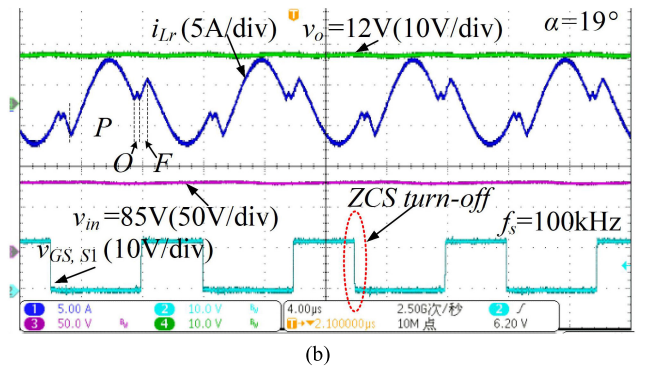
For the heavy-load condition, the voltage gain of the LLC converter is decreased along with the load increasing, as shown in Fig. 2. Hence, it is urgent to improve the capability of voltage gain step-up for the LLC converter under heavy-load condition. Therefore, from Fig. 14, when the voltage ringing is higher than zero by detecting the voltages across SR switches, the LLC converter works at conventional PO mode to keep the high efficiency at the light-load condition. For the heavy load and high step-up voltage gain case, when the voltage ringing reaches to zero by detecting the voltages across SR switches, the converter can work at PF mode by using the proposed scheme to cover the wide voltage-regulation range, instead of using two-stage converters or adding some auxiliary switches to enhance the voltage-regulation capability.

When the LLC converter operates at the same input voltage, output voltage, and load current, the key waveforms are shown in Fig. 17. When the converter operates at PO mode with $\alpha = 0^\circ$ in Fig. 17(a) and POF mode with $\alpha = 19^\circ$ in Fig. 17(b), the switching frequency is increased from 56 to 100 kHz. As a sequence, the switching frequency range can be squeezed significantly along with the increased leading angle α , which is consistent with the theoretical analysis. In addition, according to Fig. 13(a), although 73-V minimum input voltage can be achieved theoretically, the partial hard switching occurred in the primary switches due to a very low current at the end of the O stage and caused the voltage spike across the primary switches, as shown in Fig. 17(a). Therefore, the actual minimum input voltage should be at least higher than 85 V, so that the switching frequency is close to the resonant frequency to increase the current at the end of the O stage and achieves ZVS turn-on of the primary switches. For this reason, the voltage regulation range of the traditional LLC converter with PO mode is further squeezed and the maximum voltage gain is around

$$G = \frac{2nV_o}{V_{in}} = \frac{2 \times 5 \times 12}{87} = 1.38. \quad (18)$$



(a)



(b)

Fig. 17. Experimental waveforms at 12-V/8-A output and 85-V input. (a) 56-kHz switching frequency under PO mode and $\alpha = 0^\circ$ and (b) 100-kHz switching frequency under POF mode and $\alpha = 19^\circ$.

As shown in Fig. 17, the peak current i_{Lr} is 6.5 A in the traditional LLC converter with PO mode from Fig. 17(a), while the peak current i_{Lr} is 5.5 A in the proposed LLC converter with POF mode from Fig. 17(b), which verifies that the peak current i_{Lr} can be reduced by the proposed F stage.

From Fig. 16(a), the primary switches are turned-on when the F stage ends. According to Fig. 17, when the primary switches are turned on, the primary current i_{Lr} is increased from 0.3 A under conventional PO mode to 3.2 A under proposed PF mode at 85-V input and 12-V/8-A output conditions. Therefore, the ZVS condition of the primary switches shown in (19) can be satisfied more easily, thereby reduced dead time of primary switches to improve the efficiency [12]

$$i_{Lr,Q_p,\text{on}} t_{\text{dead}} \geq 2C_{\text{oss},Q_p} V_{\text{in}} \quad (19)$$

where $i_{Lr,Q_p,\text{on}}$ is the resonant current when the primary switches are turned on, t_{dead} is the dead time of primary switches, and C_{oss,Q_p} is the output parasitic capacitance of the primary switches.

Fig. 18(a) shows the maximum voltage gain when the converter operates at PF mode with $\alpha = 47^\circ$, and the maximum voltage gain

$$G = \frac{2nV_o}{V_{\text{in}}} = \frac{2 \times 5 \times 12}{54} = 2.22 \quad (20)$$

with 54-V input can be achieved at 87-kHz switching frequency and 12-V/8-A output, which is corresponding with Fig. 12(a). Fig. 18(b) shows the ZVS turn-on of SR switches S_1 and S_2 PF mode with 47° leading angle, which verifies the soft

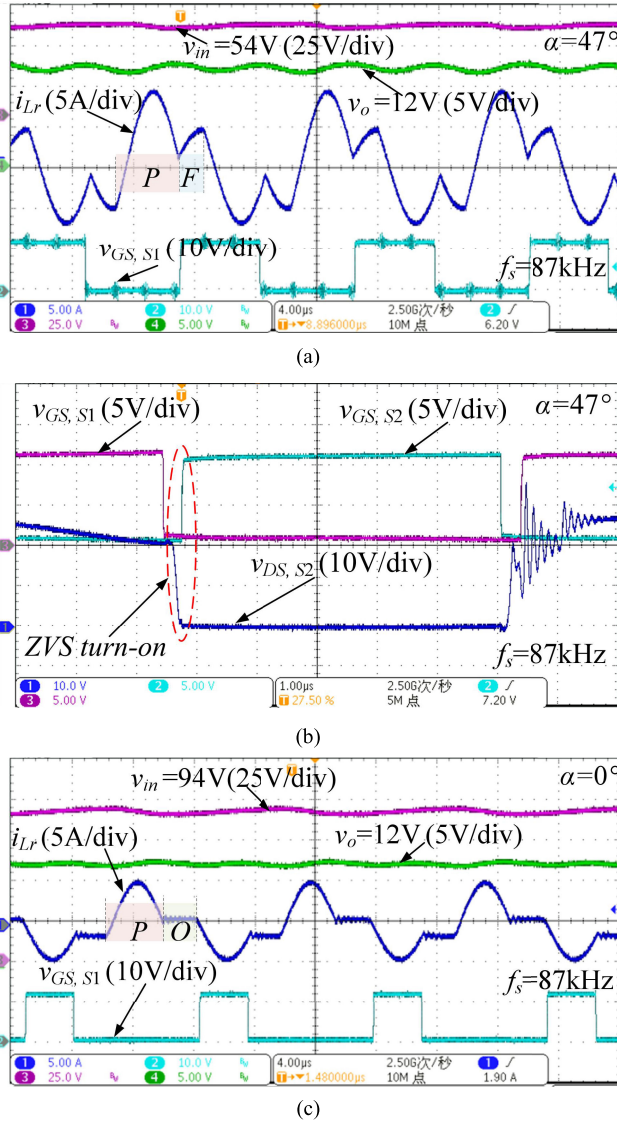


Fig. 18. Experimental waveforms at 12-V/8-A output and 87-kHz switching frequency at (a) and (b) 54-V input voltage under PF mode and $\alpha = 47^\circ$ and (c) 94-V input voltage under PO mode and $\alpha = 0^\circ$.

switching characteristic of the proposed scheme. As shown in Fig. 18(c), at the same output and switching frequency condition, the voltage gain is

$$G = \frac{2nV_o}{V_{in}} = \frac{2 \times 5 \times 12}{94} = 1.28 \quad (21)$$

with PO mode. Therefore, at the same load condition, the maximum voltage gain can be improved 1.61 times according to (18) and (20), and the voltage gain can be improved 1.73 times by the proposed novel operation modes at 87-kHz switching frequency according to (20) and (21).

Table II shows the loss analysis of the proposed converter. Fig. 19 shows the loss breakdown at different voltage-regulation ranges and load conditions. From Fig. 19, the loss proportion of the switches S_1 and S_2 at half-load is much higher than that at full-load as ZVS turn-on may not be achieved at light load, which is consistent with the theoretical analysis in [34] and experimental verification in Fig. 16. Therefore, in scenarios with heavy loads and high step-up

TABLE II
LOSS ANALYSIS OF THE PROPOSED DC–DC CONVERTER

P_{con}	$I_{Q1,rms}^2 R_{ds(on)} + I_{Q2,rms}^2 R_{ds(on)}$ ($I_{Q1,rms}$ and $I_{Q2,rms}$ are RMS value of drain-to-source current through switches Q_1 and Q_2 , $R_{ds(on)}$ is on-state resistance of primary switches)
$P_{Q1} + P_{Q2}$	$\frac{1}{2} t_f V_{in} f_s i_{Lr}(t_6) + \frac{1}{2} t_f V_{in} f_s i_{Lr}(t_2)$ (t_f is falling time of primary switches)
P_{driver}	$v_g(Q_{g1} + Q_{g2})f_s$ (v_g is drive voltage of primary switches, Q_{g1} and Q_{g2} are gate charge of switch Q_1 and Q_2)
$P_{S1} + P_{S2}$	$I_{S1,rms}^2 R_{ds(on)} + I_{S2,rms}^2 R_{ds(on)}$ ($I_{S1,rms}$ and $I_{S2,rms}$ are RMS value of drain-to-source current through switches S_1-S_2 , $R_{ds(on)}$ is on-state resistance of secondary switches)
P_{diode}	$\frac{V_F}{T_s} (\int_{t_0-td}^{t_0} i_{S1} dt + \int_{t_4-td}^{t_4} i_{S2} dt)$ (t_d is conduction time of the body diodes of secondary switches)
P_{driver}	$v_g(Q_{gs1} + Q_{gs2})f_s$ (v_g is drive voltage of secondary switches, Q_{gs1} and Q_{gs2} are gate charge of switch S_1 and S_2)
P_{Lr}	$I_{Lr}^2 R_{ac,Lr}$ ($R_{ac,Lr}$ and I_{Lr} are the AC resistance, and the AC RMS current of the inductor L_r , respectively)
P_{core}	$P_v V$ (P_v is constants, which are related to material and ΔB , V is the volume of the core of inductor L_r)
P_{Tx}	$I_{Lp}^2 R_{ac,Lp} + I_{Ls}^2 R_{ac,Ls}$ ($R_{ac,Lp}$ and I_{Lp} are the AC resistance, and the RMS current in primary side; $R_{ac,Ls}$ and I_{Ls} are the AC resistance, and the AC RMS current in secondary side)
P_{core}	$P_v V$ (P_v is constants, which are related to material and ΔB , V is the volume of the core of transformer T_x)
P_C	$I_{C_{in,rms}}^2 R_{ESR,Cin} + I_{Cr,rms}^2 R_{ESR,Cr} + I_{Co,rms}^2 R_{ESR,Co}$ ($R_{ESR,Cin}$, $R_{ESR,Cr}$ and $R_{ESR,Co}$ are equivalent series resistance of capacitors C_{in} , C_r and C_o . $I_{C_{in,rms}}$, $I_{Cr,rms}$ and $I_{Co,rms}$ are RMS value of the current through capacitors C_{in} , C_r and C_o)
<i>Auxiliary power supply</i>	Power for controller and ICs, and others (copper loss of the track, etc.)

voltage gain, the voltage-regulation range can be extended by the proposed control strategy with high efficiency.

Fig. 20 shows the measured efficiency of the PF mode LLC converter and the PO mode LLC converter under soft switching condition with the same power circuit parameters. Although the efficiency with PF mode is slightly lower than that with PO mode at 12-V/8-A output, the voltage-regulation range is much wider with PF mode; thereby, the minimum input voltage can

TABLE III
COMPARISON OF THE WIDE VOLTAGE-REGULATION RANGE *LLC* DC-DC CONVERTERS

References	[10]	[22]	[41]	[42]	This work
Wide voltage-regulation range method	Reduced k	Full bridge / half bridge morphing	Reduced L_m	Parameter optimization	SR switches turn-on early
Input voltage	320-370	220-760	220-320	370-410	54-115
Output voltage	35-165	400	28	36-72	12
Transformer ratio	22:9	1.125:1	5	4:1:1	20:4:4
Maximum voltage gain	2.52	2.05	1.24	1.57	2.22
Frequency variation range	110 kHz~320 kHz	83kHz~120kHz	792 kHz~1.12MHz	150 kHz~450 kHz	87 kHz~100 kHz
Efficiency	94%	97.8%	96%	96%	96.82%

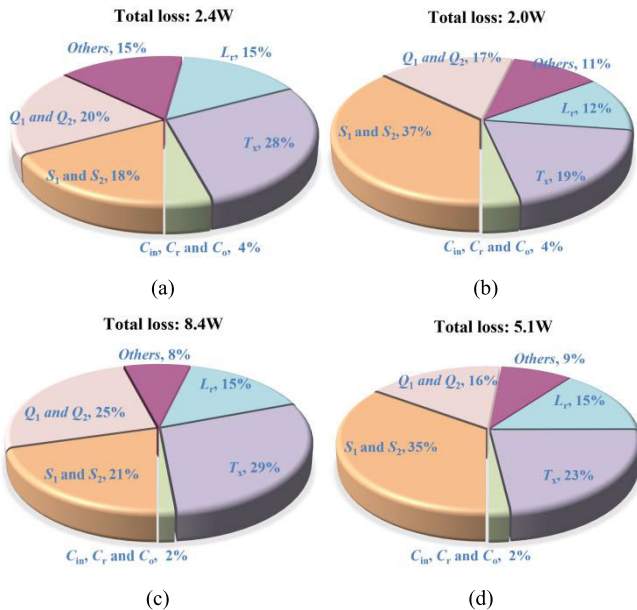


Fig. 19. Loss breakdown of the proposed converter at (a) $V_{in} = 115$ V, $V_o = 12$ V, full load, (b) $V_{in} = 115$ V, $V_o = 12$ V, half-load, (c) $V_{in} = 60$ V, $V_o = 12$ V, full load, and (d) $V_{in} = 60$ V, $V_o = 12$ V, half-load.

be extended from around 87–54 V with ZVS turn-on of all the switches.

Table III gives the comparison of the wide voltage-regulation range *LLC* dc-dc converters. From Table III, by using a large parallel resonant inductance to reduce the circulating current and achieve soft switching easier in the proposed *LLC* converter, the voltage-regulation range is extended, and the switching frequency range is squeezed without any auxiliary devices. In addition, the proposed wide-voltage-gain scheme can be adopted in any simple *LLC* resonant converter topology, and the consistent primary-side or secondary-side switching frequency keeps the temperature among these switches balanced. In summary, the proposed novel operation mode of the *LLC* converter

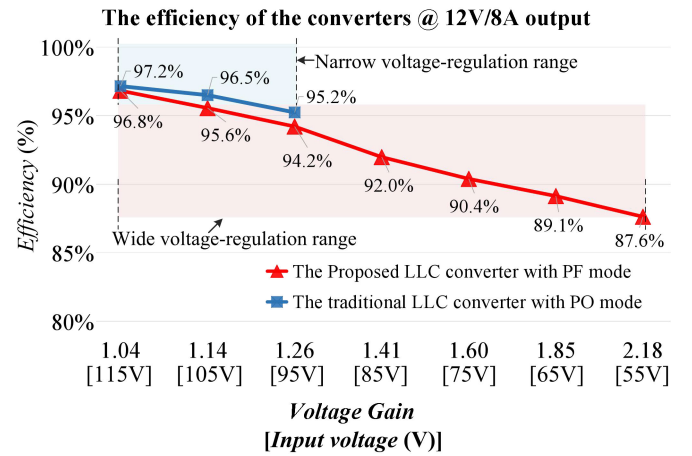


Fig. 20. Measured efficiency.

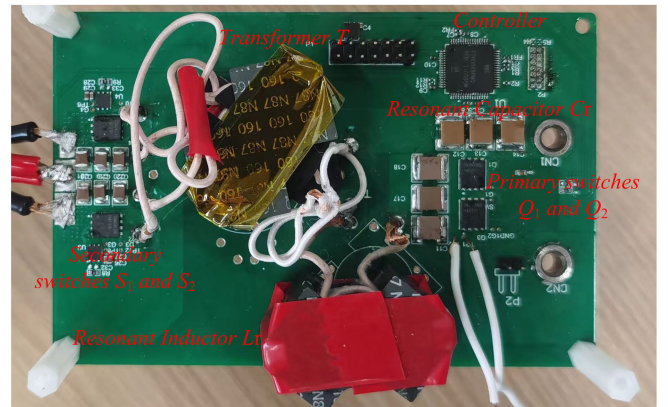


Fig. 21. Experimental prototype.

provides a simple, low-cost, and effective scheme to improve the voltage-regulation capability of the resonant converter.

Fig. 21 shows the experimental prototype of the proposed converter, and Fig. 22 shows the testing platform.

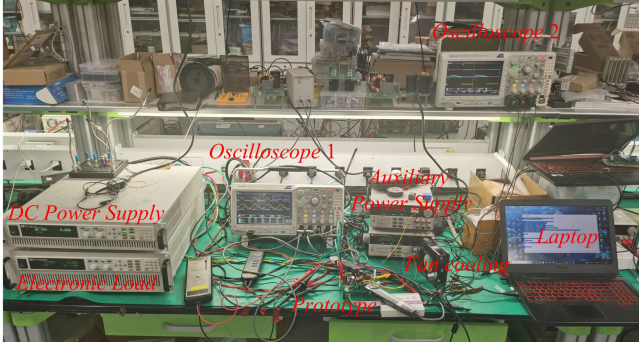


Fig. 22. Testing platform.

V. CONCLUSION

Different from the conventional SR *LLC* converter operation modes consisting of P, O, and N stages, stage F is built and the novel operation modes contained F stage are analyzed in this article. In the SR *LLC* converter with the POF or PF mode, the soft-switching of primary- and secondary-side switches can be achieved, and the advantages of the conventional *LLC* converter, such as simple circuit structure and control strategy, are kept. Along with the leading angle α increasing in the proposed operation modes, the switching frequency range is squeezed and the step-up voltage gain is improved significantly without any added components. In addition, the proposed operation modes can easily extend half-bridge *LLC* converter, full-bridge *LLC* converter, or three-level *LLC* converter, all kinds of SR *LLC* converters. Therefore, by using the proposed approach, the wide voltage-regulation range with a narrow switching frequency range can be achieved in *LLC* converter, which overcomes the drawback of *LLC* converter unsuitable for wide voltage-regulation applications.

REFERENCES

- [1] J.-W. Kim, B. Kim, D. Lee, Y. Cho, S. K. Ji, and D. Ryu, "LLC resonant converter for fast electric vehicle charging module with a reconfigurable bi-directional switch," *IEEE Trans. Transport. Electrific.*, vol. 10, no. 4, pp. 10169–10181, Dec. 2024.
- [2] B. O. Aarninkhof, D. Lyu, T. B. Soeiro, and P. Bauer, "A reconfigurable two-stage 11kW DC–DC resonant converter for EV charging with a 150–1000 V output voltage range," *IEEE Trans. Transport. Electrific.*, vol. 10, no. 1, pp. 509–522, Mar. 2024.
- [3] C. Sun, R. Wang, X. Xiao, Y. Wang, and Q. Sun, "Model-free bidirectional synchronous rectification control scheme for LLC-based energy storage system in electric-vehicle energy router," *IEEE Trans. Transport. Electrific.*, vol. 9, no. 4, pp. 5140–5150, Dec. 2022.
- [4] G. Xu, S. Luo, J. Xu, W. Xiong, Y. Sun, and M. Su, "An ISOP LLC converter with changeable equivalent magnetizing inductance utilizing coupled inductor for ultrawide input voltage range application," *IEEE Trans. Transport. Electrific.*, vol. 10, no. 2, pp. 3680–3689, Jun. 2024.
- [5] M. I. Shahzad, S. Iqbal, and S. Taib, "Interleaved LLC converter with cascaded voltage-doubler rectifiers for deeply depleted PEV battery charging," *IEEE Trans. Transport. Electrific.*, vol. 4, no. 1, pp. 89–98, Mar. 2018.
- [6] E. G. Schmidtner, "A new high-frequency resonant converter topology," in *Proc. High Freq. Power Convers. (HFPC) Conf. Rec.*, 1988, pp. 390–403.
- [7] J. F. Lazar and R. Martinelli, "Steady-state analysis of the LLC resonant converter," in *Proc. IEEE Appl. Power Electron. Conf. Expo.*, Anaheim, CA, USA, Mar. 2001, pp. 728–735.
- [8] B. Yang, F. C. Lee, A. J. Zhang, and G. Huang, "LLC resonant converter for front end DC/DC conversion," in *Proc. IEEE Appl. Power Electron. Conf. Expo.*, vol. 2, Dallas, TX, USA, Jun. 2003, pp. 1108–1112.
- [9] B. Yang, "Topology investigation for front end DC/DC power conversion for distributed power system," Ph.D. dissertation, Virginia Tech Center Power Electron. Syst., Virginia Polytech. Inst. State Univ., Blacksburg, VA, USA, 2003.
- [10] R. Beiranvand, B. Rashidian, M. R. Zolghadri, and S. M. H. Alavi, "A design procedure for optimizing the LLC resonant converter as a wide output range voltage source," *IEEE Trans. Power Electron.*, vol. 27, no. 8, pp. 3749–3763, Aug. 2012.
- [11] X. Fang et al., "Efficiency-oriented optimal design of the LLC resonant converter based on peak gain placement," *IEEE Trans. Power Electron.*, vol. 28, no. 5, pp. 2285–2296, May 2013.
- [12] Y. Wei, Q. Luo, Z. Wang, and H. A. Mantooth, "A complete step-by-step optimal design for LLC resonant converter," *IEEE Trans. Power Electron.*, vol. 36, no. 4, pp. 3674–3691, Apr. 2021.
- [13] X. Fang, H. Hu, Z. J. Shen, and I. Batarseh, "Operation mode analysis and peak gain approximation of the LLC resonant converter," *IEEE Trans. Power Electron.*, vol. 27, no. 4, pp. 1985–1995, Apr. 2012.
- [14] X. Zhou et al., "A high-efficiency high-power-density on-board low-voltage DC–DC converter for electric vehicles (EVs) application," *IEEE Trans. Power Electron.*, vol. 36, no. 11, pp. 12781–12794, Nov. 2021.
- [15] R. Beiranvand, B. Rashidian, M. R. Zolghadri, and S. M. H. Alavi, "Using LLC resonant converter for designing wide-range voltage source," *IEEE Trans. Ind. Electron.*, vol. 58, no. 5, pp. 1746–1756, May 2011.
- [16] Z. Fang, T. Cai, S. Duan, and C. Chen, "Optimal design methodology for LLC resonant converter in battery charging applications based on time-weighted average efficiency," *IEEE Trans. Power Electron.*, vol. 30, no. 10, pp. 5469–5483, Oct. 2015.
- [17] A. Mustafa and S. Mekhilef, "Dual phase LLC resonant converter with variable frequency zero circulating current phase-shift modulation for wide input voltage range applications," *IEEE Trans. Power Electron.*, vol. 36, no. 3, pp. 2793–2807, Mar. 2021.
- [18] T. Qian and C. Qian, "A combined topology with coupled LLC resonance for wide-range operation," *IEEE Trans. Power Electron.*, vol. 34, no. 7, pp. 6593–6600, Jul. 2019.
- [19] B. Xue, H. Wang, J. Liang, Q. Cao, and Z. Li, "Phase-shift modulated interleaved LLC converter with ultrawide output voltage range," *IEEE Trans. Power Electron.*, vol. 36, no. 1, pp. 493–503, Jan. 2021.
- [20] H. Wang, Y. Chen, P. Fang, Y.-F. Liu, J. Afsharian, and Z. Yang, "An LLC converter family with auxiliary switch for hold-up mode operation," *IEEE Trans. Power Electron.*, vol. 32, no. 6, pp. 4291–4306, Jun. 2017.
- [21] I.-H. Cho, Y.-D. Kim, and G.-W. Moon, "A half-bridge LLC resonant converter adopting boost PWM control scheme for hold-up state operation," *IEEE Trans. Power Electron.*, vol. 29, no. 2, pp. 841–850, Feb. 2014.
- [22] D. Sha and X. Yang, "Wide voltage input full bridge(FB)/half bridge(HB) morphing-based LLC DC–DC converter using numerical optimal trajectory control," *IEEE Trans. Ind. Electron.*, vol. 70, no. 4, pp. 3697–3707, Apr. 2023.
- [23] Y. Wei, Q. Luo, and H. A. Mantooth, "An LLC converter with multiple operation modes for wide voltage gain range application," *IEEE Trans. Ind. Electron.*, vol. 68, no. 11, pp. 11111–11124, Nov. 2021.
- [24] C. Li, M. Zhou, and H. Wang, "An H5-bridge-based asymmetric LLC resonant converter with an ultrawide output voltage range," *IEEE Trans. Ind. Electron.*, vol. 67, no. 11, pp. 9503–9514, Nov. 2020.
- [25] X. Tang, Y. Xing, H. Wu, and J. Zhao, "An improved LLC resonant converter with reconfigurable hybrid voltage multiplier and PWM-plus-PFM hybrid control for wide output range applications," *IEEE Trans. Power Electron.*, vol. 35, no. 1, pp. 185–197, Jan. 2020.
- [26] H. Wu, Y. Li, and Y. Xing, "LLC resonant converter with semi-active variable-structure rectifier (SA-VSR) for wide output voltage range application," *IEEE Trans. Power Electron.*, vol. 31, no. 5, pp. 3389–3394, May 2016.
- [27] P. Rehlaender, O. Wallscheid, F. Schafmeister, and J. Böcker, "LLC resonant converter modulations for reduced junction temperatures in half-bridge mode and transformer flux in the on-the-fly morphing thereto," *IEEE Trans. Power Electron.*, vol. 37, no. 11, pp. 13413–13427, Nov. 2022.
- [28] H. Hu, X. Fang, F. Chen, Z. J. Shen, and I. Batarseh, "A modified high-efficiency LLC converter with two transformers for wide input-voltage range applications," *IEEE Trans. Power Electron.*, vol. 28, no. 4, pp. 1946–1960, Apr. 2013.
- [29] D. Shu and H. Wang, "An ultrawide output range LLC resonant converter based on adjustable turns ratio transformer and reconfigurable bridge," *IEEE Trans. Ind. Electron.*, vol. 68, no. 8, pp. 7115–7124, Aug. 2021.

- [30] J.-W. Kim and G.-W. Moon, "A new LLC series resonant converter with a narrow switching frequency variation and reduced conduction losses," *IEEE Trans. Power Electron.*, vol. 29, no. 8, pp. 4278–4287, Aug. 2014.
- [31] K.-W. Kim, H.-S. Youn, J.-I. Baek, Y. Jeong, and G.-W. Moon, "Analysis on synchronous rectifier control to improve regulation capability of high-frequency LLC resonant converter," *IEEE Trans. Power Electron.*, vol. 33, no. 8, pp. 7252–7259, Aug. 2018.
- [32] Z. Fang et al., "Energy feedback control of light-load voltage regulation for LLC resonant converter," *IEEE Trans. Power Electron.*, vol. 34, no. 5, pp. 4807–4819, May 2019.
- [33] S. Bagawade, M. Pahlevani, and P. Jain, "Novel resonant power feedback DC–DC converter," *IEEE Trans. Power Electron.*, vol. 38, no. 3, pp. 4072–4091, Mar. 2023.
- [34] X. Zhou, L. Wang, Y. Gan, H. Luo, Y.-F. Liu, and P. C. Sen, "Accurate analysis and design of the circuit parameters of LLC DC–DC converter with synchronous rectification," *IEEE Trans. Power Electron.*, vol. 37, no. 12, pp. 15051–15065, Dec. 2022.
- [35] *MnZn Ferrite Material (EPCOS N87) Datasheet*, U.S. Dept. Energy Natl. Energy Technol. Lab., Pittsburgh, PA, USA, Sep. 2018.
- [36] Y. Li, Q. Wu, L. Liu, and Z. Zhu, "An adaptive constant voltage control scheme for primary-side controlled flyback converter," *IEEE Trans. Ind. Electron.*, vol. 70, no. 7, pp. 6776–6785, Jul. 2023.
- [37] J. Zhang, H. Zeng, and X. Wu, "An adaptive blanking time control scheme for an audible noise-free quasi-resonant flyback converter," *IEEE Trans. Power Electron.*, vol. 26, no. 10, pp. 2735–2742, Oct. 2011.
- [38] C. Wang, S. Xu, W. Shen, S. Lu, and W. Sun, "A single-switched high-switching-frequency quasi-resonant flyback converter," *IEEE Trans. Power Electron.*, vol. 34, no. 9, pp. 8775–8786, Sep. 2019.
- [39] J. Park et al., "Quasi-resonant (QR) controller with adaptive switching frequency reduction scheme for flyback converter," *IEEE Trans. Ind. Electron.*, vol. 63, no. 6, pp. 3571–3581, Jun. 2016.
- [40] H.-P. Park and J.-H. Jung, "Modeling and feedback control of LLC resonant converters at high switching frequency," *J. Power Electron.*, vol. 16, no. 3, pp. 849–860, May 2016.
- [41] A. de Juan, D. Serrano, P. Alou, J.-N. Mamousse, R. Deniéport, and M. Vasic, "High-frequency LLC converter with narrow frequency variations for aircraft applications," in *Proc. IEEE Appl. Power Electron. Conf. Expo. (APEC)*, Mar. 2022, pp. 2098–2105.
- [42] F. Musavi, M. Craciun, D. S. Gautam, W. Eberle, and W. G. Dunford, "An LLC resonant DC–DC converter for wide output voltage range battery charging applications," *IEEE Trans. Power Electron.*, vol. 28, no. 12, pp. 5437–5445, Dec. 2013.



Xiang Zhou (Senior Member, IEEE) received the B.S. and Ph.D. degrees in electrical engineering from Southwest Jiaotong University, Chengdu, China, in 2013 and 2018, respectively.

From June 2018 to December 2019, he was with the Department of Electrical and Computer Engineering, Queen's University, Kingston, ON, Canada, as a Post-Doctoral Research Fellow. Since 2019, he has been with Xi'an Jiaotong University, Xi'an, where he is currently an Associate Research Fellow with the School of Electrical Engineering. His research interests include soft switching dc–dc and dc–ac converter topology and control strategy and high-efficiency high-power-density converter design with wide bandgap devices.

research interests include soft switching dc–dc and dc–ac converter topology and control strategy and high-efficiency high-power-density converter design with wide bandgap devices.



Jiarui Wu (Student Member, IEEE) was born in Sichuan, China, in 1996. He received the B.S. degree in electrical engineering and automation from Northeast Forestry University, Harbin, China, in 2019, and the Ph.D. degree in electrical engineering from Xi'an Jiaotong University, Xi'an, China, in 2024.

His main research interests include high-frequency magnetics and high-power density converter.



Huan Luo (Member, IEEE) received the B.S. degree in electrical engineering from Southwest Jiaotong University, Chengdu, China, in 2012, and the M.S. degree in electrical engineering from Sichuan University, Chengdu, in 2015, and the Ph.D. degree in electrical engineering from Southwest Jiaotong University, in 2020.

He is currently an Associate Professor with the College of Electrical Engineering, Sichuan University. His research interests include the control technique of switching-mode power supplies, single-phase power factor correction, and resonant converters.



Zihao Song was born in Shandong, China, in 2001. He received the B.S. degree in electrical engineering from Harbin Institute of Technology, Harbin, Weihai, China, in 2024. He is currently pursuing the M.S. degree with Xi'an Jiaotong University, Xi'an, China.

His research interests include soft switching dc–dc converter and dc–ac converter topology and control.



Long Pei (Student Member, IEEE) was born in Hunan, China, in 1995. He received the B.S. degree in electrical automation from Xi'an Jiaotong University, Xi'an, China, in 2018, where he is currently pursuing the Ph.D. degree in electrical engineering and automation.

His research interests include on-board charge, design and control of dc–dc resonant power converters, and power factor correction ac–dc converters.



Donghua Duan (Student Member, IEEE) was born in Jiangxi, China, in 2000. He received the B.S. degree in electrical automation from Xi'an Jiaotong University, Xi'an, China, in 2022, where he is currently pursuing the M.S. degree in electrical engineering and automation.

His research interests include the design and control of dc–dc resonant power converters, machine learning and intelligent systems and applications, and big data applications.



Peng Guo (Member, IEEE) was born in Hunan, China, in 1992. He received the B.S. degree in electrical engineering from Wuhan University of Technology, Wuhan, China, in 2015, and the Ph.D. degree in electrical engineering from Hunan University, Changsha, China, in 2020.

From 2020 to 2023, he was a Post-Doctoral Fellow with Hunan University, where he is currently an Associate Professor with the College of Electrical and Information Engineering. His research interests include switch-mode power amplifier, data-driven nonlinear control, electromagnetic sensing, and electromagnetic compatibility for high-frequency power electronics systems.



Laili Wang (Senior Member, IEEE) received the B.S., M.S., and Ph.D. degrees from the School of Electrical Engineering, Xi'an Jiaotong University, Xi'an, China, in 2004, 2007, and 2011, respectively.

Since 2011, he has been a Post-Doctoral Research Fellow with the Department of Electrical Engineering, Queen's University, Kingston, ON, Canada. From 2014 to 2017, he was an Electrical Engineer with Sumida, Kingston. In 2017, he became a Full Professor with Xi'an Jiaotong University. He has published more than 240 papers in IEEE journals

and conferences and has been issued 45 Chinese patents and five U.S. patents. His research interests include wide bandgap power semiconductors, packaging and integration, and high-density power conversion.

Dr. Wang has been rewarded the Gold Medal Award of Geneva Inventions, the First Prize Award of Science and Technology Progress of China Power Supply Society (CPSS), the First Prize of Technical Invention of China Electrotechnical Society (CES), and the Second Prize Award of Natural Science of Shaanxi Province. He was a recipient of the National Science Fund for Distinguished Young Scholars, Shaanxi Youth Science and Technology Award, the Outstanding Youth Award of China Power Supply Society (CPSS), the Youth Science and Technology Award of China Electrotechnical Society (CES), and China Electric Power Excellent Young Technological Talent Award of Chinese Society of Electrical Engineering (CSEE). He is currently an Associate Editor of IEEE TRANSACTIONS ON POWER ELECTRONICS and IEEE JOURNAL OF EMERGING AND SELECTED TOPICS IN POWER ELECTRONICS. He is the Co-Chair of System Integration and Application in International Technology Roadmap for Wide Band-Gap Power Semiconductor (ITRW), the Chair of IEEE PELS and CPSS Joint Chapter in Xi'an, and the Vice Chair of IEEE PELS Membership Committee-China. He is also the Vice Chair of the four committees in China Power Supply Society (CPSS).



Yan-Fei Liu (Fellow, IEEE) received the bachelor's and master's degrees from the Department of Electrical Engineering, Zhejiang University, Hangzhou, China, in 1984 and 1987, respectively, and the Ph.D. degree from the Department of Electrical and Computer Engineering, Queen's University, Kingston, ON, Canada, in 1994.

He was a Technical Advisor with the Advanced Power System Division, Nortel Networks, Ottawa, ON, Canada, from 1994 to 1999. Since 1999, he has been with Queen's University, where he is currently

a Professor with the Department of Electrical and Computer Engineering. He has authored around 250 technical papers in IEEE transactions and conferences and holds 35 U.S. patents. He has written a book on "*High Frequency MOSFET Gate Drivers: Technologies and Applications*," published by IET. His current research interests include optimal application of GaN and SiC devices to achieve small size and high-efficiency power conversion, 99% efficiency power conversion with extremely high power density, digital control technologies for high efficiency, fast dynamic response dc–dc switching converter and ac–dc converter with power factor correction, resonant converters and server power supplies, and LED drivers.

Dr. Liu is also a Principal Contributor for two IEEE standards. He received the "Modeling and Control Achievement Award" from IEEE Power Electronics Society in 2017. He received the Premier's Research Excellence Award in ON, Canada, in 2000. He also received the Award of Excellence in Technology in Nortel in 1997. He serves as an Editor for IEEE JOURNAL OF EMERGING AND SELECTED TOPICS OF POWER ELECTRONICS (JESTPE) since 2013. He was the Vice President of Technical Operations of IEEE Power Electronics Society (PELS) from 2017 to 2020. He was the General Chair of ECCE 2019 held in Baltimore, USA, in 2019. His major service to IEEE is listed as follows: a Guest Editor-in-Chief for the special issue of Power Supply on the Chip of IEEE TRANSACTIONS ON POWER ELECTRONICS from 2011 to 2013; a Guest Editor for special issues of JESTPE: Miniaturization of Power Electronics Systems in 2014 and Green Power Supplies in 2016; the Co-General Chair of ECCE 2015 held in Montreal, Canada, in September 2015; the Chair of PELS Technical Committee (TC1) on Control and Modeling Core Technologies from 2013 to 2016; and the Chair of PELS Technical Committee (TC2) on Power Conversion Systems and Components from 2009 to 2012.